Energy and enstrophy fluxes in the double cascade of 2d turbulence

G. Boffetta

Dipartimento di Fisica Generale and INFN, Università degli Studi di Torino, Via Pietro Giuria 1, 10125, Torino, Italy
and CNR-ISAC, Sezione di Torino, Corso Fiume 4, 10133 Torino, Italy
(Dated: August 13, 2018)

High resolution direct numerical simulations of two-dimensional turbulence in stationary conditions are presented. The development of an energy-enstrophy double cascade is studied and found to be compatible with the classical Kraichnan theory in the limit of extended inertial ranges. The analysis of the joint distribution of energy and enstrophy fluxes in physical space reveals a small value of cross correlation. This result supports many experimental and numerical studies where only one cascade is generated.

PACS numbers:

The existence of two quadratic inviscid invariants is the most distinguishing feature of Navier Stokes equations in two dimensions. On this basis, in a remarkable paper in 1967 [1], Kraichnan predicted the double cascade scenario for two-dimensional turbulence: an inverse cascade of kinetic energy $E = 1/2\langle v^2 \rangle$ to large scales and a direct cascade of enstrophy $Z = 1/2\langle \omega^2 \rangle$ to small scales ($\omega = \boldsymbol{\nabla} \times \boldsymbol{v}$ is the vorticity). In statistically stationary conditions, when the turbulent flow is sustained by an external forcing acting on a typical scale ℓ_f a double cascade develops. According to the Kraichnan theory, at large scales i.e. wavenumbers $k \ll k_f \sim \ell_f^{-1}$, the energy spectrum has the form $E(k) \simeq \varepsilon^{2/3} k^{-5/3}$, while at small scales, $k \gg k_f$, the prediction is $E(k) \simeq \eta^{2/3} k^{-3}$, with a possible logarithmic correction [2]. Here ε and $\eta \simeq k_f^2 \varepsilon$ are respectively the energy and the enstrophy injection rate.

Despite the importance of two-dimensional turbulence as a model for many physical flows [3, 4] and, more in general, for non-equilibrium statistical systems [5], a clear evidence of the coexisting two cascades on an extended range of scales is still lacking. The inverse energy cascade has observed in many laboratory experiments [6] and in numerical simulations [7, 8, 9] with a statistical accuracy which has revealed the absence of intermittency corrections to the dimensional scaling [10]. For what concerns the direct cascade, earlier numerical simulations and experiments report spectra slightly steeper than k^{-3} [11, 12], while more recent investigations at high resolution are closer to Kraichnan prediction [13, 14, 15, 16]. It is important to remark that in presence of a large scale drag force (always present in experiments and sometimes also in numerics) one indeed expects a correction to the classical exponent -3 [17, 18].

Two recent experimental papers have been devoted to the study of the double cascade [19, 20]. Their results are substantially consistent with the classical scenario of Kraichnan, although the extension of the inertial range (in particular for the inverse cascade) is limited. Here we present high resolution (up to 16384^2) direct numerical simulations of forced 2D Navier-Stokes equations which reproduce with good accuracy both the cascades simultaneously. Most of the injected energy flows to large scales (where it is removed by friction dumping) while enstrophy cascades to small scales (there removed by viscosity). We find strong numerical indications that the classical Kraichnan scenario is recovered in the limit of two extended inertial ranges, although we are unable to rule our the possibility of small corrections in the direct cascade. By looking at the two fluxes in physical space, we find a relatively small value of the cross correlation among them. This result is interpreted in favor of the possibility of generating a single cascade, independently on the presence of the second inertial range.

The 2D Navier-Stokes equation for the vorticity field is

$$\partial_t \omega + \boldsymbol{v} \cdot \boldsymbol{\nabla} \omega = \nu \Delta \omega - \alpha \omega + \Delta f, \qquad (1)$$

where ν is the kinematic viscosity and α is a linear friction coefficient (representing bottom friction or air friction) necessary to obtain a stationary state. The forcing term f is assumed to be short correlated in time (in order to control the injection rates) and narrow banded in space. Specifically, we use a Gaussian forcing with correlation function $\langle f(\boldsymbol{r}, t) f(\boldsymbol{0}, 0) \rangle = \delta(t) F \ell_f^2 exp(-(r/\ell_f)^2/2)$ in most of the simulations. For the simulations at resolution 16384 we use a different forcing restricted to a narrow shell of wavenumbers. Numerical integration of (1) is performed by pseudo-spectral, fully dealiased, parallel code on a doubly periodic square domain at resolution N^2. Statistical quantities are computing by averaging over several large-scale eddy turnover times in stationary conditions (only over a fraction of eddy turnover time for the 16384 run because of limited resources). Table I reports the most important parameters of our simulations.

One of the simplest information which can be obtained from Table I is related to the energy-enstrophy balance. At $N = 2048$ only about one half of the energy injected is transfered to large scales where it is removed by friction at a rate $\varepsilon_\alpha = 2\alpha E$. This fraction increases with the resolution and becomes about 95 % for the $N = 16386$ run. The remaining energy injected is dissipated by viscosity

N	ν	α	ℓ_f/ℓ_d	$\varepsilon_\alpha/\varepsilon_I$	$\varepsilon_\nu/\varepsilon_I$	η_α/η_I	η_ν/η_I
2048	2×10^{-5}	0.015	26.2	0.54	0.46	0.03	0.97
4096	5×10^{-6}	0.024	52.3	0.82	0.18	0.08	0.92
8192	2×10^{-6}	0.025	80.5	0.92	0.08	0.10	0.90
16384	1×10^{-6}	0.03	114.2	0.95	0.05	0.12	0.88

TABLE I: Parameters of the simulations. N spatial resolution, ν viscosity, α friction, L box size, $\ell_f = L/100$ forcing scale, $\ell_d = \nu^{1/2}/\eta_\nu^{1/6}$ enstrophy dissipative scale, ε_I energy injection rate, ε_ν viscous energy dissipation rate, ε_α friction energy dissipation rate, η_I enstrophy injection rate, η_ν viscous enstrophy dissipation rate, η_α friction enstrophy dissipation rate.

at scales comparable with the forcing scale and at a rate proportional to ν (which thus decreases by increasing the resolution).

On the other side, most of the enstrophy (around 90 %) follows the direct cascade to small scales, where it is dissipated by viscosity. We observe a moderate increase of the large scale enstrophy dissipation η_α increasing the resolution: this is a finite-size effect due the increase of α with N (see Table I) necessary to keep the friction scale $\ell_\alpha \simeq \varepsilon_\alpha^{1/2}\alpha^{-3/2}$ constant with increasing ε_α.

In Figure 1 we plot the fluxes of energy and enstrophy in wavenumber space. Observe that because change the resolution keeping the ratio L/ℓ_f constant, the only effect of reducing the resolution on the inverse cascade is the decrease of the energy transferred to large scales (being $\varepsilon_\alpha = \varepsilon_I - \varepsilon_\nu$ with ε_ν proportional to ν) while the extension of the inertial range is almost unaffected. The qualitative difference at $k \simeq k_f$ for the run at $N = 16384$ is due to the different forcing implemented in this case, while statistical fluctuations are a consequence of the short time statistics. These results confirm the robustness of the energy inertial range regardless of the viscous dissipative scale, a further justification of many simulations of the inverse cascade in which, because of the limited resolution, the forcing scale is very close to the dissipative scale.

At variance with the inverse cascade, the direct enstrophy cascade is strongly affected by finite resolution effects. This is not a surprise because, by keeping ℓ_f fixed, the extension of the direct cascade is simply proportional to N. As it is shown in Figure 1, we observe a range of wavenumbers with almost constant flux $\Pi_Z(k)$ only for the runs at $N \geq 8192$.

Figure 2 shows the energy spectra computed for the different runs. We remark again that the only effect of finite resolution on the inverse cascade is the reduction of the energy transfered to large scales, while the Kolmogorov scaling $k^{-5/3}$ is always observed with a Kolmogorov constant $C \simeq 6$ [10] virtually independent on resolution. The effect of finite resolution is, of course, more dramatic on the enstrophy cascade range. We observe here a significative correction to the Kraichnan spectrum k^{-3}
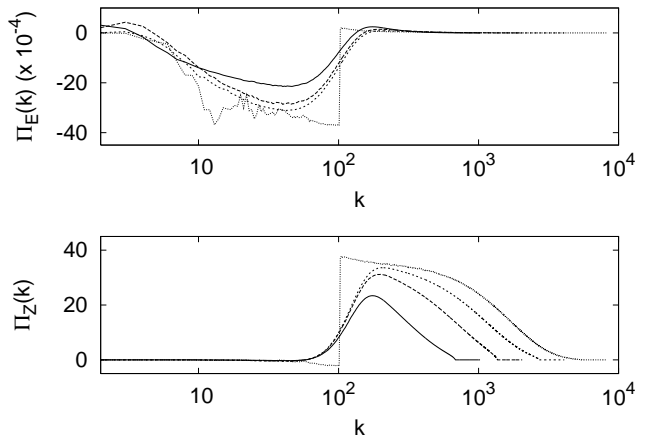

FIG. 1: Energy (top) and enstrophy (bottom) fluxes in Fourier space at resolutions 2048, 4096, 8192 and 16384. Resolution increases from smaller to larger absolute values of the minimum/maximum. At resolution 16384 statistics is computed on a single frame.

even for the 16384 run, where measure a scaling exponents close to -3.6. We remark a similar steepening of the spectrum has been observed even for simulations with a more resolved direct cascade range (here we have $k_{max}/k_f \simeq 55$ at the highest resolution). Despite these difficulties, there is a clear indication that the correction to the exponent is a finite-size effect which eventually disappears by increasing the extension of the inertial range (see inset of Fig. 2). The conclusion of these considerations is that a k^{-3} spectrum in stationary solutions of (1) could be achieved only by taking simultaneously the limits $L/\ell_f \to \infty$ and $\ell_f/\ell_d \to \infty$ (i.e. for vanishing α and ν).

A better understanding of the physical mechanism of the cascades can be obtained by looking at the distribution of fluxes in space. This can be obtained by using a filtering procedure recently introduced and applied separately to the direct [21] and to the inverse [22] cascades. Thanks to the resolution of the present simulations, we are able to analyze jointly both the cascade and the correlations among them. Following [21], we introduce a large-scale vorticity field $\omega_r \equiv G_r \star \omega$ obtained from the convolution of ω with a Gaussian filter G_r, and a large-scale velocity field $\boldsymbol{v}_r \equiv G_r \star \boldsymbol{v}$. From these definitions, balance equations for the large-scale energy $e_r(\boldsymbol{x},t) = 1/2|\boldsymbol{v}_r|^2$ and enstrophy $z_r(\boldsymbol{x},t) = 1/2\omega_r^2$ densities are easily written (with a compact notation):

$$\partial_t(e_r, z_r) + \boldsymbol{\nabla} \cdot \boldsymbol{J}_r^{(e,r)} = -\Pi_r^{(e,r)} - D_r^{(e,r)} + F_r^{(e,r)} \quad (2)$$

where $\boldsymbol{J}_r^{(e,z)}$ represent the transport of large-scale energy and enstrophy, $D_r^{(e,z)}$ and $F_r^{(e,r)}$ represent the large-scale dumping and forcing. The energy/enstrophy fluxes $\Pi_r^{(e,z)}(\boldsymbol{x},t)$, representing the local transfer of energy/enstrophy from large scale to scales smaller than r,
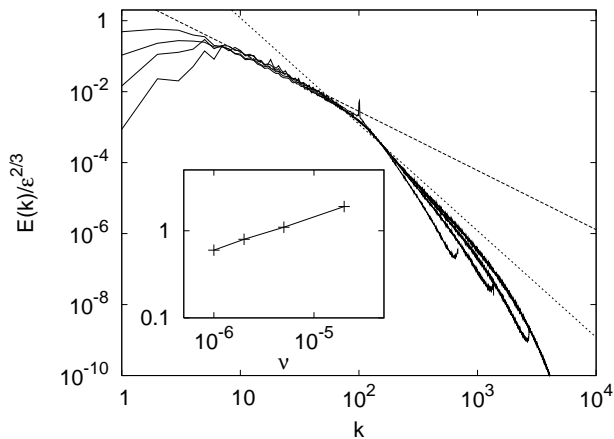
FIG. 2: Energy spectra for the two simulations for the different resolutions (resolution increases with the extension of the tail). Dashed and dotted lines represent the two predictions $Ck^{-5/3}$ with $C = 6$ and k^{-3} respectively. Inset: correction to the Kraichnan exponent -3 measured in the range $100 \leq k \leq 400$ as a function of viscosity.

are given by:

$$\Pi_r^{(e)}(\boldsymbol{x}, t) \equiv -(\tau_{\alpha\beta})_r \nabla_\alpha (v_\beta)_r \qquad (3)$$

$$\Pi_r^{(z)}(\boldsymbol{x}, t) \equiv -(\sigma_\alpha)_r \nabla_\alpha \omega_r \qquad (4)$$

where $(\tau_{\alpha\beta})_r = (v_\alpha v_\beta)_r - (v_\alpha)_r (v_\beta)_r$ and $(\sigma_\alpha)_r = (v_\alpha \omega)_r - (v_\alpha)_r \omega_r$.
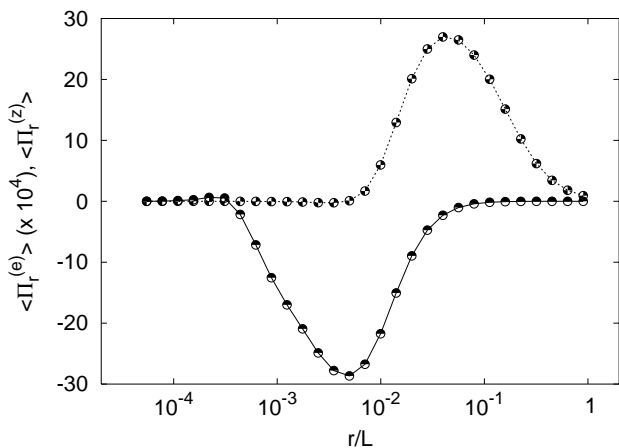

FIG. 3: Average energy (lower, continuous) and enstrophy (upper, dotted) fluxes in physical space at resolution $N = 8192$. The energy flux is multiplied by a factor $k_f^2 = 10^4$ for better visualization.

Fluxes (3-4) are expected to have a non-zero spatial mean in the inertial range of scales of irreversible turbulent cascades: in particular a mean negative energy flux for $r > \ell_f$ (inverse cascade) and a mean positive enstrophy flux for $r < \ell_f$ (direct cascade). Figure 3 shows the averaged physical fluxes $\langle \Pi_r^{(e,z)} \rangle$ as functions of the scale

r. The two cascades are evident, although the range of constant flux is reduced with respect to the spectral case in both the cascades (see Fig. 1).

Local fluxes are strongly inhomogeneous in physical space: there are relatively small regions of intense (positive and negative) flux in both the energy and enstrophy inertial ranges. Figure 4 shows two snapshots of the energy and enstrophy fluxes, computed from the same field at two different scales r_1 and r_2 corresponding to the minimum of energy flux and the maximum of enstrophy flux respectively (see Fig. 3). An interesting information, obtained from Fig. 4 at a qualitative level, is that the most intense energy and enstrophy fluxes appear on different physical region without any apparent correlation.
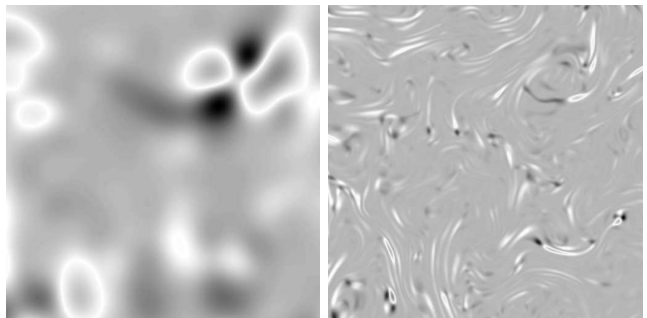

FIG. 4: Snapshot of energy (left) and enstrophy (right) fluxes from the same vorticity field. Energy flux (3) is computed at scale $r_1 = 0.025L$ and enstrophy flux at $r_2 = 0.0025L$, roughly corresponding to the minimum and maximum in Fig. 3. White and black correspond to positive and negative values respectively.

Figure 4 shows that both positive and negative fluxes are observed: locally both energy and enstrophy can go to smaller or larger scales. Figure 5 shows the probability density functions of the two fluxes. As observed in previous studies [21, 22], the shapes of pdf's are nearly symmetric, confirming the qualitative picture inferred from Fig. 4. The mean values in both cases is the result of strong cancellations as its ratio with the standard deviation is -0.22 for the energy flux and 0.16 for the enstrophy flux. The skewness is also small as it is about 0.9 and 1.2 for the energy and enstrophy fluxes respectively.

Figure 6 shows the joint probability density function $p(\Pi_{r_1}^{(e)}, \Pi_{r_2}^{(z)})$ for the same scales r_1 and r_2. This pdf is not far from the product of the marginal distributions shown in Fig. 5, a condition for independence. Indeed, the cross correlation among $\Pi_{r_1}^{(e)}$ and $\Pi_{r_2}^{(z)}$ is only $C(r_1, r_2) \simeq -0.15$. Of course, it is very different if we consider the correlation at the same scale, for which we find $C(r, r) \simeq 1$ despite the fact that one of the fluxes has zero mean. A possible interpretation of the observed small value of correlation is in favor of the classical picture of independence of the two cascades which is here obtained at a local level. Therefore, our result is, a posteriori, a support to many experimental and numerical
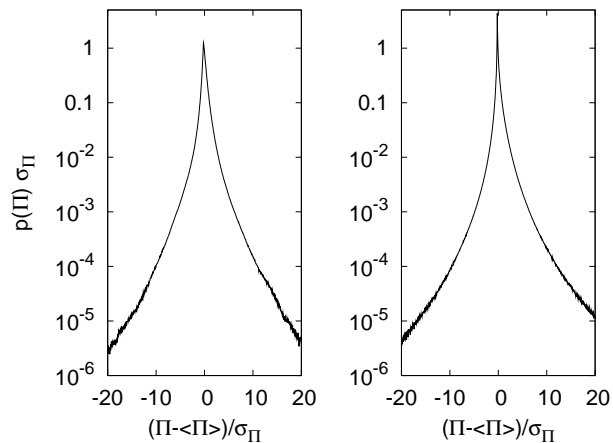
FIG. 5: Probability density function of energy $\Pi_{r_1}^{(e)}$ (left) and enstrophy $\Pi_{r_2}^{(e)}$ (right) fluxes normalized with their standard deviations. Resolution is $N = 8192$, filtering scales are $r_1 = 0.025L$ and $r_2 = 0.0025L$.

studies in which, due to finite size constraints, only one cascade is realized.
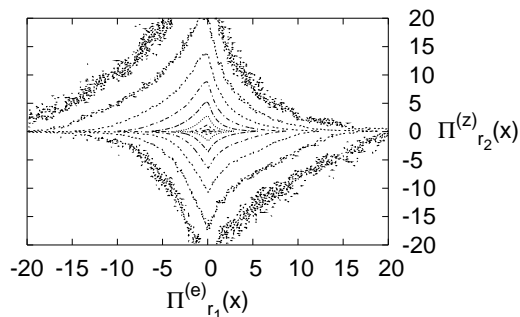

FIG. 6: Joint probability density function $p(\Pi_{r_1}^{(e)}, \Pi_{r_2}^{(z)})$ of energy (x-axis) and enstrophy (y-axis) fluxes. Scales r_1 and r_2 as in Fig. 5. Contours are plotted on a logarithmic scale while fluxes are normalized with their standard deviations.

In conclusion, we have presented statistical analysis of high resolution direct numerical simulations of 2D Navier-Stokes equations which clearly reproduce, for the first time, the double cascade scenario predicted by Kraichnan almost 40 years ago.

Simulations were performed on the IBM-CLX cluster of Cineca (Bologna, Italy) and on the *Turbofarm* cluster at the INFN computing center in Torino.

[1] R.H. Kraichnan, *Inertial Ranges in Two-Dimensional Turbulence* Phys. Fluids **10**, 1417, (1967).

[2] R.H. Kraichnan, *Inertial-range transfer in two- and three-dimensional turbulence* J. Fluid Mech. **47**, 525, (1971).

[3] R.H. Kraichnan and D. Montgomery, *Two-dimensional turbulence* Rep. Prog. Phys., **43**, 547, (1980).

[4] P. Tabeling, *Two-dimensional turbulence: a physicist approach* Phys. Rep. **362**, 1, (2002).

[5] D. Bernard, G. Boffetta, A. Celani and G. Falkovich, *Conformal invariance in two-dimensional turbulence* Nature Phys. **2**, 124, (2006).

[6] J. Paret and P. Tabeling, *Experimental Observation of the Two-Dimensional Inverse Energy Cascade* Phys. Rev. Lett. **79**, 4162, (1997).

[7] E. Siggia and H. Aref, *Point-vortex simulation of the inverse energy cascade in two-dimensional turbulence* Phys. Fluids **24**, 171, (1981).

[8] U. Frisch and P.L. Sulem, *Numerical simulation of the inverse cascade in two-dimensional turbulence* Phys. Fluids **27**, 1921, (1984).

[9] L. Smith and V. Yakhot, *Bose condensation and small-scale structure generation in a random force driven 2D turbulence* Phys. Rev. Lett. **71**, 352, (1993).

[10] G. Boffetta, A. Celani and M. Vergassola, *Inverse energy cascade in two-dimensional turbulence: Deviations from Gaussian behavior* Phys. Rev. E **61**, R29 (2000).

[11] B. Legras, P. Santangelo and R. Benzi, *High-Resolution Numerical Experiments for Forced Two-Dimensional Turbulence* Europhys. Lett. **5**, 37 (1988).

[12] H. Kellay, X.L. Wu and W.I. Goldburg, *Experiments with Turbulent Soap Films* Phys. Rev. Lett. **74**, 3975 (1995).

[13] V. Burue, *Spectral exponents of enstrophy cascade in stationary two-dimensional homogeneous turbulence* Phys. Rev. Lett. **71**, 3967 (1993).

[14] T. Gotoh, *Energy spectrum in the inertial and dissipation ranges of two-dimensional steady turbulence* Phys. Rev. E **57**, 2984 (1998).

[15] E. Lindborg and K. Alvelius, *The kinetic energy spectrum of the two-dimensional enstrophy turbulence cascade* Phys. Fluids **12**, 945 (2000).

[16] C. Pasquero and G. Falkovich, *Stationary spectrum of vorticity cascade in two-dimensional turbulence* Phys. Rev. E **65**, 056305 (2002).

[17] K. Nam, E. Ott, T.M. Antonsen and P.N. Guzdar, *Lagrangian Chaos and the Effect of Drag on the Enstrophy Cascade in Two-Dimensional Turbulence* Phys. Rev. Lett. **84**, 5134 (2000).

[18] G. Boffetta, A. Celani, S. Musacchio and M. Vergassola, *Intermittency in two-dimensional Ekman-Navier-Stokes turbulence* Phys. Rev. E **66**, 026304 (2002).

[19] M.A. Rutgers, *Forced 2D Turbulence: Experimental Evidence of Simultaneous Inverse Energy and Forward Enstrophy Cascades* Phys. Rev. Lett. **81**, 2244 (1998).

[20] C.H. Bruneau and H. Kellay, *Experiments and direct numerical simulations of two-dimensional turbulence* Phys. Rev. E **71**, 046305 (2005).

[21] S. Chen, R.E. Ecke, G.L. Eyink, X. Wang and Z. Xiao, *Physical Mechanism of the Two-Dimensional Enstrophy Cascade* Phys. Rev. Lett. **91**, 214501 (2003).

[22] S. Chen, R.E. Ecke, G.L. Eyink, M. Rivera, M. Wan and Z. Xiao, *Physical Mechanism of the Two-Dimensional Inverse Energy Cascade* Phys. Rev. Lett. **96**, 084502 (2006).